

# Abstract

Theoretical condensed matter research is plagued by a fundamental issue of complexity. The sheer amount of degrees of freedom in a material on any technologically relevant scale is overwhelming (e.g.  $\sim 10^{23}$  electrons per  $\text{cm}^3$ ), and makes it impossible to describe the quantum mechanical wavefunction exactly.

The Hamiltonian plays a central role in the description of crystals, the subject of this thesis. It can be decomposed into various parts, and their interactions. Depending on the physics under scrutiny it then often suffices to solve only one of those parts. This can be either because the energy scales and associated timescales that govern the constituents are very different, or because the interactions between them are small. One example, often put into practice, is the separation of electronic and phononic (lattice) degrees of freedom, leading to the well-known Born-Oppenheimer approximation, decoupling their respective motion. Another is the often neglected spin-orbit coupling, due to the tiny prefactor associated with its relativistic origin.

Solving these subproblems then allows for progress to be made in understanding the physics that govern them. However, there will inevitably be systems for which this interaction is not small and leads to fascinating new physics that manifestly depends on both subsystems combined. In this thesis we focus on these cases and how they arise in functional materials, with the occasional eye towards applications in technology.

The reason why these cross-order couplings can be interesting for technological applications, is that often one of the orders is more robust with respect to perturbations, and therefore more long-lived, but also harder to control efficiently. By exploiting the cross-order coupling in certain materials, one could potentially control the long lived order by applying perturbations to the more easily controllable order.

In giant Rashba effect systems, the coupling between spin and ferroelectric order leads to a linear spin-splitting of the band structure, whose sign depends on the orientation of the ferroelectric polarization. We show that, rather than the relativistic Rashba effect, a combination of electrostatics and atomic spin-orbit coupling lies at the origin of the large splitting.

The coupling between magnetism and ferroelectricity in multiferroic  $\text{GdMn}_2\text{O}_5$  leads to a never before observed four-state hysteresis loop for the ferroelectric polarization, which depends on the magnitude, angle and history of the applied magnetic field. As we will show, this four-state hysteresis loop is accompanied by a full  $360^\circ$  rotation of spins in the material, which resembles the crankshaft of a car, converting the linear back-and-forth motion of the magnetic field into a rotational motion of the spins.

In a thin film of elemental Chromium, the ultrafast dynamics of a spin

density wave, coupled to a slower varying charge density wave, allows for a high degree of control of the latter through excitations of the former. This allows us to predict the sequence of optical pulses to be applied to the material in order to follow closely an enveloping signal function.

And finally, the coupling between ferroelectricity and strain in BaTiO<sub>3</sub> leads to a softening at purely ferroelectric domain walls, allowing for some mechanical control of the position of this wall.

We utilize both theoretical and computational tools to understand the nature of these interactions, how they lead to cross-order coupling in these materials, and how this then translates into the experimentally observed behavior.

# Chapter 1

## Coupling between spin and strain density waves

### 1.1 Introduction

In all previous chapters, we discussed situations for which the order parameters were static, or at least at equilibrium. For GeTe, the polarization and resulting spin splitting was fixed. Even though it is interesting to study what the effect of changes to the polarization has to this splitting [Monserrat2017], even in that case, the electrons can be assumed to be in equilibrium with the changing potential at all times. This is because the electronic dynamics is so much faster than the atomic ones, meaning that the Born-Oppenheimer approximation is still valid. In the study on GdMn<sub>2</sub>O<sub>5</sub>, the changing magnetic structure and corresponding ferroelectric polarization was orders of magnitude faster than the change of the magnetic field, again allowing an equilibrium description. However, the regime in which this breaks down is certainly accessible to experiments with faster varying magnetic fields. In the case of BaTiO<sub>3</sub> with the softening domain wall, while the experiments were dependent on a resonance frequency, the applied perturbation was found to not markedly change the properties of the material, warranting again a static description. New physics arise, however, when two orders with different timescales for their dynamics are coupled, and where the slave order parameter has slower dynamics than the primary one. This is the case in the material we study here, Chromium, an itinerant antiferromagnetic metal [Kulikov1984, Fawcett1988]. It is the hallmark example of a material where a spin density wave (SDW) develops due to local repulsive interactions of the electron gas, combined with a nesting of the fermi surface. Due to magnetostriction, this spin density wave then causes a periodic lattice displacement (PLD) which decreases the bondlengths between the spins that have large magnitude. The SDW is formed by electrons and thus thermalizes on very quick timescales when a perturbation is applied[Nicholson2016]. The coupled PLD, however, denotes the movement of atoms and thus has much slower dynamics. With ultrafast pump-probe experiments that have a below picosecond resolution, these PLD dynamics can be studied and, more importantly, controlled very precisely through excitation of the much faster responding SDW. Among other things, this allows for the suppression of the intermediate nonequilibrium state

and reproducing adiabatic transitions on much faster timescales than would be possible without this control, which is termed “shortcuts to adiabaticity” in quantum technology [**Torronegui2013**, **Deffner2014**, **Zhou2017**]. This also allows to apply a specifically designed set of pulses in order for the PLD oscillation to follow a particular envelope function, as will be shown theoretically below.

## 1.2 Experimental methods

Before focusing on the theoretical description of the coupling between the SDW and PLD, we take a look at the experimental techniques employed by A. Singer’s group and the results that we are seeking to reproduce. A thin film (28 nm) of Cr was used, supporting around seven periods of the SDW with a Néel temperature  $T_N$  of 290 K, slightly lower than in the bulk where  $T_N \approx 308$  K. The film was illuminated by two sequential 40 fs optical pulses at times  $\tau_1$  and  $\tau_2$ , heating up the electronic subsystem and the SDW which is a part of it. Due to magnetostriction, this SDW is coupled with a PLD which is probed through the Bragg peaks by an x-ray free-electron laser (XFEL)[**Singer2015**]. XFELs allow for high peak selectivity (narrow and intense satellite Bragg peaks), making measurements performed on thin films even deposited on thick substrates accessible. The scattering intensity of the Bragg peak is directly proportional to the magnitude of the PLD, offering both phase and amplitude information of the PLD oscillation that occurs when the SDW is (partially) melted by the optical pulses. The high resolution ultrafast measurements that the XFEL enables (fs timescales), allows to follow the evolution of the PLD in time. The acoustic phonon associated with the PLD oscillation has a wavevector normal to the material surface and an oscillation time period of approximately 450 fs. The heat exchange rate between the lattice (or bath) and the electrons is quite high, leading to a thermalization between the two subsystems within a picosecond after heating. Even though some heat is deposited in the system, and the heat capacity is not infinite, the final temperature stays below the Néel temperature leading to a recovery of the SDW and eventually the PLD, as can be seen by the non-zero oscillation equilibrium at the end of the measurements in Fig. ???. Due to the slight increase in temperature of the system (around 45 K), this equilibrium amplitude of the PLD is slightly lower after the pulses, compared with before. The damping time of the PLD is around 3 ps. Further thermalization of the Cr lattice to the substrate occurs on the nanosecond timescale, out of the scope of our measurements. It is important to realize that the SDW order is not directly accessible through these kinds of measurements, so we are effectively studying the effect of exciting one order parameter through the reaction of the other by the coupling between them.

The most interesting observation is that by changing the timing of the second pulse  $\tau_2$ , the dynamics of the PLD can be controlled to a high degree. In Fig. ??(b-c) it can be seen that the oscillation amplitude in the first one is almost completely destroyed by the second pulse, whereas in panel c it is increased slightly. Panel a of the same figure shows a more complete visualization of this effect, where the horizontal bands with low amplitude signify the destructive interference and those with high amplitude the constructive situation.

The maximum PLD amplitude that is reached in the experiments, after the

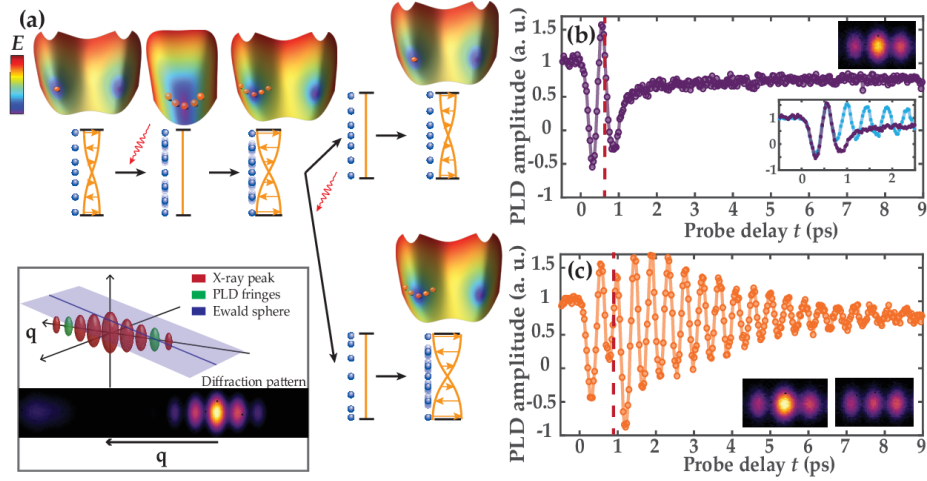


**Figure 1.1: Controlled enhancement and destruction of the excited state.** (a) A laser pulse excites the system by destroying the magnetic order; a second pulse either excites the released phonon further or stops the excitation. Schematic energy surfaces show the PLD state as the orange point. Inset: x-ray scattering from periodic atomic displacement is detected on a fringe of the main peak from the crystalline film. (b-c) Amplitude of the PLD in two extreme control cases. Solid lines are experimental data (empty circles) - connected. The dashed red line marks the time of second pulse arrival. (b)  $\tau_2 - \tau_1 = 620$  fs, (c)  $\tau_2 - \tau_1 = 845$  fs. Insets show the Laue fringe with the satellite peak at maximum and minimum PLD values.

second pulse is 150% of the original amplitude. This is significantly higher than the excitation amplitudes associated with the conventional displacive excitation mechanism, where the ratio is about one [Singer2015, Zeiger1992]. When the second pulse arrives before the SDW had time to cool down, the maximum oscillation amplitude is lowered as can be seen from the horizontal band around  $\tau_2 - \tau_1 = 0$  ps in Fig. ??(a). As will be further discussed below, this signifies that the SDW exceeds  $T_N$ , and some of the heating does not contribute to a larger excitation of the PLD phonon.

Experiments performed at higher fluence, i.e. such that the SDW gets heated and stays above  $T_N$  from a single pulse, show that the second pulse does not impact the oscillation of the PLD, and the influence of its timing is completely lost, as can be seen from Fig. ??(c). If control is the goal, it is thus important that the SDW is allowed to cool down below  $T_N$ . The SDW order parameter varies the most with temperature when it is close to the critical point, increasing the pulse efficiency. The XFEL also demonstrates the absence of topological defects by the absence of a widening of the satellite peak associated with the PLD, as compared with the peaks of the material itself, supporting the assumption that through the use of a thin film, the optical pulses excite the material homogeneously.

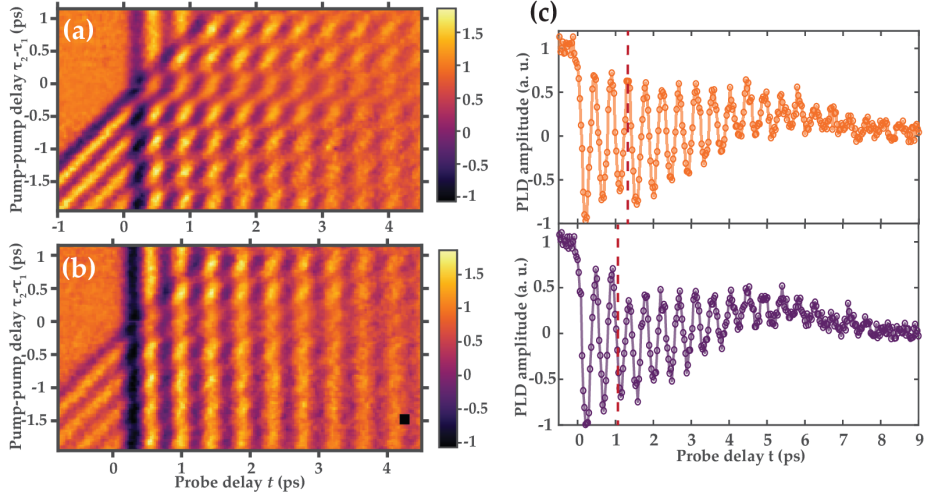


Figure 1.2: **Experimental maps of the excited state depending on probe and pump delay.** (a) Map of the PLD amplitude before and after excitation by two pulses with a fluence of  $1.45 \text{ mJ/cm}^2$ . (b) Same as (a) but with the second pulse twice less intense than the first. (c) Magnitude of the PLD in “enhancement” and “suppression” conditions at laser pulse fluence of  $9.5 \text{ mJ/cm}^2$  for the first and  $4.7 \text{ mJ/cm}^2$  for the second. The dashed line marks the arrival time of the second pulse,  $\tau_2 - \tau_1 = 1295 \text{ fs}$  for the top panel and  $1065 \text{ fs}$  for the bottom.

### 1.3 Theory

[some explanation of Peierls instabilities etc, the things that cause the SDW in the first place?]

As was already alluded to, we can describe the effect of the photon pulses by considering two subsystems with two temperatures. The first is the electronic subsystem, that thermalizes on a 100 fs timescale, as was shown by high-resolution ARPES measurements [**Nicholson2016**], and can thus be considered to be always thermal on the picosecond timescales that we are interested in, allowing us to assign a temperature to it. The SDW is formed by electronic states and thus belongs to the electronic subsystem [**Nicholson2016**], with the same temperature  $T_L$ . The second subsystem is the lattice (phonon modes excluding the mode associated with the PLD) which we denote as the bath which is always assumed to be thermal, with temperature  $T_b$ . After the electronic system absorbs the heat from the pulses, it will exchange heat with this bath, cooling it down within one picosecond. This process can be described by the so-called two temperature model:

$$\begin{aligned} C_L \dot{T}_L &= -k(T_L(t) - T_b(t)) + Q_p h(t) \\ C_b \dot{T}_b &= -k(T_b(t) - T_L(t)), \end{aligned} \quad (1.1)$$

with  $k$  the heat transfer rate,  $C_L$  and  $C_b$  the heat capacities of the electronic degrees of freedom and bath, respectively. The dots signify time derivatives. As one could expect, we find that the heat capacity of the bath is larger than

that of the electronic system by an order of magnitude[ref]. Finally, the heat injected by the pulses is modelled by a gaussian  $Q_{ph}(t) = Ae^{\frac{-(t-\tau)^2}{\xi^2}}$ , with  $A$  the strength,  $\tau$  the duration and  $\tau$  the time delay.

The changes to  $T_L$  through heating and subsequent cooling affects the amplitude SDW order parameter ( $L$ ) and indirectly the one describing the PLD ( $y$ ), as described by a Landau-type theory [Khomskii2010]. These order parameters are related to the Fourier component of the SDW with wavevector  $q$ , i.e.  $L = S_q$ , and to the acoustic phonon amplitude  $y = u_{2q}$ . The phonon mode is the second harmonic ( $2q$ ) of the SDW because the magnetostriction acts on the magnitude of the spins, and not the phase, so that during one period of the SDW oscillation two periods of the PLD occur. This leads to the following expression for the total free energy:

$$F(L, y, T_L) = \frac{\alpha}{2}(T_L - T_c)L^2 + \frac{\beta}{4}L^4 - gL^2y + \frac{\omega_0}{2}y^2 + \frac{b}{4}y^4, \quad (1.2)$$

where  $L$ ,  $y$  and  $T_L$  are the time dependent variables. The double well potential that leads to the SDW phase transition is characterised by  $\alpha$  and  $\beta$ , and critical temperature  $T_c$  below which the SDW order sets in. The magnetostrictive coupling between the two order parameters is described by term with  $g$ . Only even orders of  $L$  appear in the free energy, since the energy is time reversal even, but  $L$  is time reversal odd. The PLD order parameter  $y$  has a zero equilibrium value without the presence or interaction with  $L$ , since it is not the primary order parameter. The fourth order term  $\frac{b}{4}y^4$  is only included to provide a better fit to some of the anisotropic features of observed by the experiment, not to bound the energy potential in terms of  $y$ , as would be required if  $y$  was the primary order parameter with a negative second order coefficient, like in the case of  $L$ . It is the interaction with the primary order parameter  $L$  that provides the “force” to move  $y$  up in its own potential, leading to the nonzero equilibrium value. While this sounds trivial, this concept is the key to understanding the observed physics.

The time evolution of the system can be described using the Langrangian:

$$\mathcal{L}(L, y, \dot{L}, \dot{y}, t) = \frac{m_L \dot{L}(t)^2}{2} + \frac{m_y \dot{y}(t)^2}{2} - F(L, y, t), \quad (1.3)$$

with associated Euler-Lagrange equations:

$$\begin{aligned} \frac{\partial \mathcal{L}}{\partial L} - \frac{d}{dt} \frac{\partial \mathcal{L}}{\partial \dot{L}} &= \gamma_L \dot{L} \\ \frac{\partial \mathcal{L}}{\partial y} - \frac{d}{dt} \frac{\partial \mathcal{L}}{\partial \dot{y}} &= \gamma_y \dot{y} \end{aligned} \quad (1.4)$$

where the  $\gamma$  denote the damping parameters for both order parameters. Substituting Eq. ?? leads to

$$\begin{aligned} m_L \ddot{L} &= -\alpha(T_L - T_c)L - \beta L^3 - \gamma_L \dot{L} + 2gLy \\ m_y \ddot{y} &= -\omega_0^2 y - by^3 - \gamma_y \dot{y} + gL^2. \end{aligned} \quad (1.5)$$

These equations, together with Eqs. ?? describing the temperature evolution of the SDW ( $T_L$ ) under influence of the optical pulses, fully describe the dynamics

that are experimentally observed. One obvious remark can be made here, in that to be completely exact, the energy dissipated through the damping terms in Eq. ?? should be absorbed into the bath and thus influence  $T_b$ . However, the case can be made that since this is only a single mode, its contribution to the heating of the bath will be negligible compared with the one due to the thermalization of all the electronic degrees of freedom.

## 1.4 Methods

To solve the time evolution of  $L$  and  $y$  through the differential equations in Eqs. ?? we used the numerical integration methods implemented in the DifferentialEquations.jl package [**rackauckas2017differentialequations**]. More specifically the Tsit5 algorithm was used, which has adaptive timestepping to capture the sharp pulses. Originally the dynamics were fully solved both for  $L$  and  $y$ , but it was found during the fitting process that the dynamics of  $L$  are significantly faster than those of  $y$ , i.e. both the “mass” of the SDW order is orders of magnitude smaller than that for  $y$  parameter, and the parameters describing the Landau free energy potential are orders of magnitude larger (see Fig. ??). This all leads to the SDW almost perfectly tracking its instantaneous minimum on the timescales that are of interest. Solving dynamics with significantly different timescales is in general hard from the numerical point of view, and while there are other ways around this, we opted to take  $m_L = 0$  and use the instantaneous minimum in the equation describing the dynamics of  $y$ . This minimum is found by minimizing the Landau free energy in Eq. ?? for a given  $y$  and  $T_L$  in terms of  $L$ , i.e.  $\frac{\partial F}{\partial L} = 0$ , leading to:

$$L(t) = \pm \sqrt{\frac{-\alpha(T_L - T_c) + 2gy}{\beta}}. \quad (1.6)$$

The starting temperature of the bath was fixed at 115 K, and  $T_c$  was taken as 290 K, the reason for which was discussed above. Most parameters of the model described above were not known a priori and thus had to be fitted to the experimental measurements. To aid with the fitting, judicious starting values could be chosen for some parameters. For example, it was known that the pulse width  $\tau$  was under 100 fs, the oscillation frequency of the PLD  $\omega_0 \approx 14$  or equivalently a period of around 450 fs. It was also known that in general the second pulse had a fluency of around 80% that of the first, and we also chose the initial heat capacities for the bath and electronic degrees of freedom to have a ratio  $\frac{c_b}{c_L}$  on the order of 7, which was known from previous experiments [[citation](#)].

For each set of trial parameters, the time evolution of the system was solved on an interval of -2 ps to 8 ps, where the lower bound is chosen so that the numerical integration starts from a completely equilibrium initial condition. This is needed because when the sharp pulse arrives around 0 ps, some energy already enters the system slightly before 0 ps due to the gaussian shape. The error of the solution  $\tilde{x}$  w.r.t. the experimental measurements  $x$  is then the mean square sum  $err = \sum_{i=1}^n \frac{(x_i - \tilde{x}_i)^2}{n}$ , where  $i$  denote the measurement points. The numerical optimization was done through the Optim.jl package [**mogensen2018optim**],

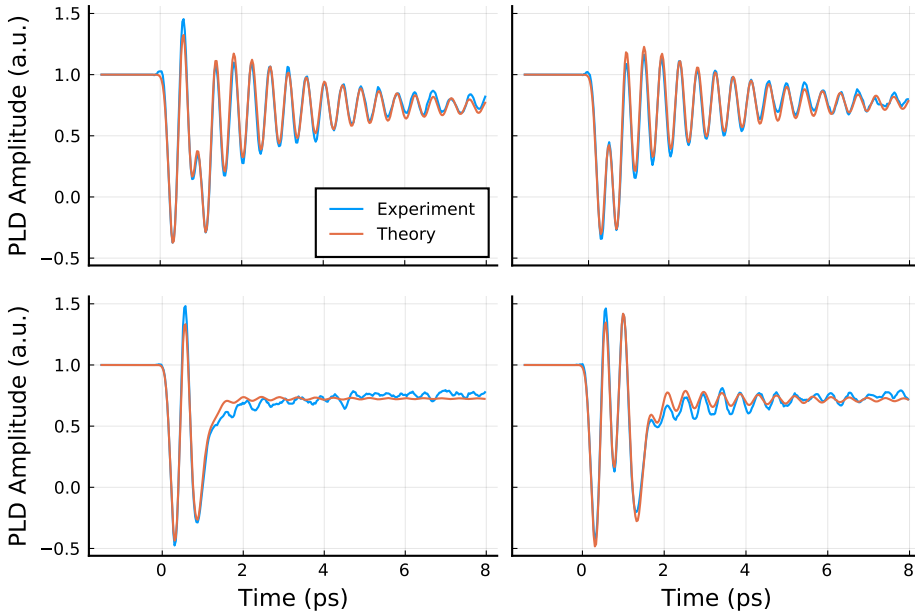


Figure 1.3: **Comparison of theoretical fit vs Experiment.** (a-b) Two examples of fits to constructive experiments. (c-d) The same for destructive interference.

where it was found that the Nelder Mead simplex algorithm [Nelder1965] works best for this very non-linear problem.

## 1.5 Results

The experimental results we use as a basis to fit our model to are shown in Fig. ???. We took eleven representative experiments, which can be thought of as horizontal slices of Fig. ??(a), in order to fit the model parameters to get the best total fit accross all datasets, allowing only the pulse fluence to fluctuate between sets. The parameters are

$$\alpha = 6.93 \cdot 10^5 \frac{eV}{K}, \beta = 6.98 \times 10^9 eV, g = 57 eV, \quad (1.7)$$

$$\frac{\omega_0}{2\pi} = 2.24 THz, b = 5.22 \times 10^{10} eV, m_y = 100 a.m.u., \gamma_y = 71.3 \frac{a.m.u.}{ps} \quad (1.8)$$

$$C_b = 3.38 \frac{eV}{K}, C_L = 0.29 \frac{eV}{K}, k = 1.3 \frac{eV}{K \cdot ps}, \xi = 86 fs, A = \frac{80}{\xi \sqrt{2\pi}} \frac{eV}{ps} \quad (1.9)$$

The results of this fitting procedure is shown in Fig. ??, showing an excellent agreement between the theory and experiment, accross the board.

To get a deeper understanding of the underlying effect, we look at the evolution of the free energy surfaces for both order parameters, as shown in Fig. ???. The characteristic double well potential for  $L \neq 0$  equilibrium is clearly visible, and as expected, when the pulses hit and  $T_L$  increases in the term  $\alpha(T_L - T_c)L^2$  of Eq. ??, we see that the potential flattens causing the the minimum of  $L$  to very

quickly change, as discussed above. This in turn causes the single-well potential of  $y$  to shift as quickly. An oscillation of  $y$  will occur due to its relatively slow dynamics, and instantaneous shift of its energy landscape as  $L$  varies. While the temperature  $T_L$  decreases again,  $L$  and the minimum of the  $y$  potential shift back towards the original equilibrium position. The oscillation of  $y$  remains for quite a long time while this shift is occurring since the damping is not that big (of the order of 4ps).

This presents us already with the first hint at the benefit of indirectly exciting the PLD through the SDW. In a hypothetical system where the PLD is the primary order parameter, and no other coupled order parameters are present, the only possibility to excite a similar oscillation is to heat it up. This would shift the minimum of the hypothetical energy potential to 0, and again due to the slow dynamics an oscillation would occur. However, as with any normal oscillator, the amplitude of the oscillation would never exceed the starting value, as the thermalization, and restoration of the potential will occur on much longer timescales. Here, however, due to the relatively fast thermalization of the SDW with the bath, the potential surface for  $y$  recovers on a faster timescale than it would on its own, leading to a relative movement of the potential opposite to the movement of  $y$  itself. This relative movement transfers additional momentum to  $y$  as the SDW is thermalizing and the potential is being restored, leading ultimately to a higher oscillation amplitude, even when only a single pulse is applied. This was observed experimentally in previous measurements by A. Singer's group and reported in Ref. [Singer2015].

One final remark to make w.r.t. to the behavior after a single pulse, is that since it is the position or magnitude of  $L$  which is the driver of the energy surface of  $y$ , the effect is most efficiently generated when  $L$  is close to  $T_c$  because a small change in temperature causes a large variation of the equilibrium position of  $L$  as shown by Eq. ?? and corresponding familiar graph in Fig. ??[make an image of general sqrt(T-Tc) behavior].

Having multiple pulses that can rapidly change the potential surface for  $y$  of course opens up many more possibilities, allowing for additional constructive interference (Fig. ??(a-b)) or, by shifting the potential surface in the same direction as the movement of  $y$ , complete destructive interference (see Fig. ??(c-d)). This can be leveraged by applying a whole train of pulses in order to create any graph your heart desires. Having this understanding, we continue by investigating what can be achieved with a longer pulse train.

First we discuss the strategy to achieve maximal amplitude. The maximal change in the value of  $L$ , and thus the potential surface for  $y$ , can be achieved by heating it all the way to  $T_c$ . It is then important to keep this initial shift of the potential for  $y$  in place until  $y$  crosses the minimum, converting as much potential energy into kinetic energy. This can be achieved by heating  $L$  to slightly above  $T_c$ , where the additional heat and finite cooling rate will keep the potential shift present until  $y$  passes through the minimum, gaining the most momentum. Fig. ?? demonstrates this by the red peaks of  $T_L$  which signify that it is above  $T_c$ . Exactly at this point  $L$  should start to reform causing the potential surface of  $y$  to start moving in the opposite direction to its movement, which in the end supplies it with additional momentum, as was described above in relation to the larger than 100% relative amplitude of  $y$  after one pulse. Since the sign of  $L$  does not matter for the position of the potential surface of  $y$ , it can only cause a shift in one direction, meaning that, similar to someone pushing a

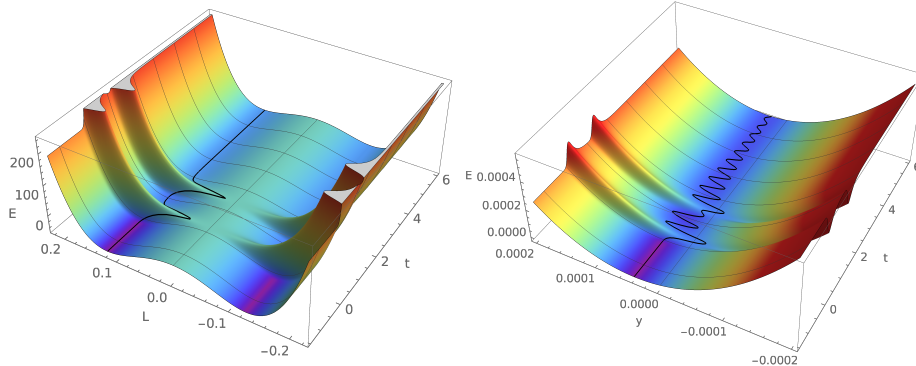


Figure 1.4: Time evolution of the energy surfaces of the order parameters.

swing, the ideal intervals for the subsequent pulses are close to multiples of the period of  $y$ , if the goal is maximum oscillation amplitude. The amount of periods depends on the cooling rate of  $L$ , and damping rate of  $y$ . The former influences how much  $T_L$  can cool back down within one period and thus the size of the maximum kinetic energy gain of  $y$ , while the latter is the main source of kinetic energy loss. From our simulations, unless the damping is really negligible, it is always best to supply a set of pulses at each oscillation period of  $y$ . The results in Fig. ?? showcase this situation, where the heat capacity of the bath was artificially increased to infinity to mimic a possible strong cooled regime which would be ideal for maximizing the oscillation amplitude. With the damping rate of  $y$  taken as in the experiment, the maximal amplitude thus achieved is about 450% the original value, quite a remarkable increase.

We can go one step further, however, and design a pulse train such that the oscillation amplitude follows a particular “signal” envelope function, demonstrating the incredibly high degree of control of the PLD that this system allows for. To limit the dimensionality of the manifold of possible solutions, we followed the ruleset:

- Only one fluence can be used per pulse
- Pulses are grouped in sets per period of oscillation
- The first pulse group only has a single pulse, purely for technical reasons
- The maximum allowed pulses per group is fixed
- The groups are then fitted sequentially, since the later pulses don’t influence the oscillation caused by the earlier ones

Adhering to these rules, we tested this procedure on different envelope functions, showcased in Fig. ???. Similar to before, the assumption of an infinite  $C_b$  was made here, this is done so the equilibrium position of  $L$  does not change, otherwise causing a general downwards slope of the oscillation of  $y$  as seen from the lower final equilibrium positions of  $y$  in panels (a-b) of Fig. ???. This showcases that with a carefully chosen pulse train we can achieve indirect, but optimal control of the PLD order parameter.

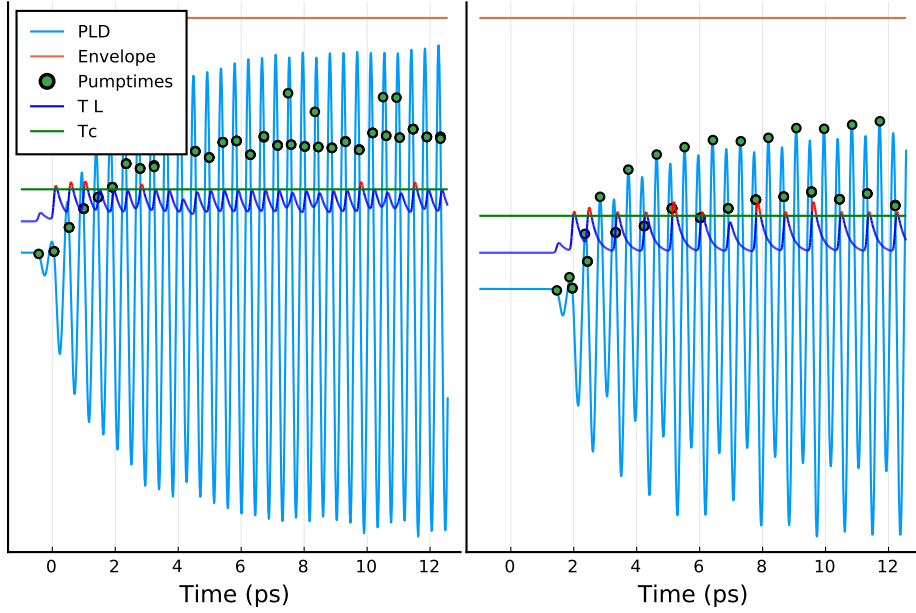


Figure 1.5: **Two schemes for achieving maximum amplitude.** (a) One set of pulses is applied within each period. (b) One set of pulses every two periods. The damping is clearly the limiting factor and warrants as many pulses per timeframe in order to achieve the maximum amplitude. In both figures, the envelope function is at 450% the original magnitude.

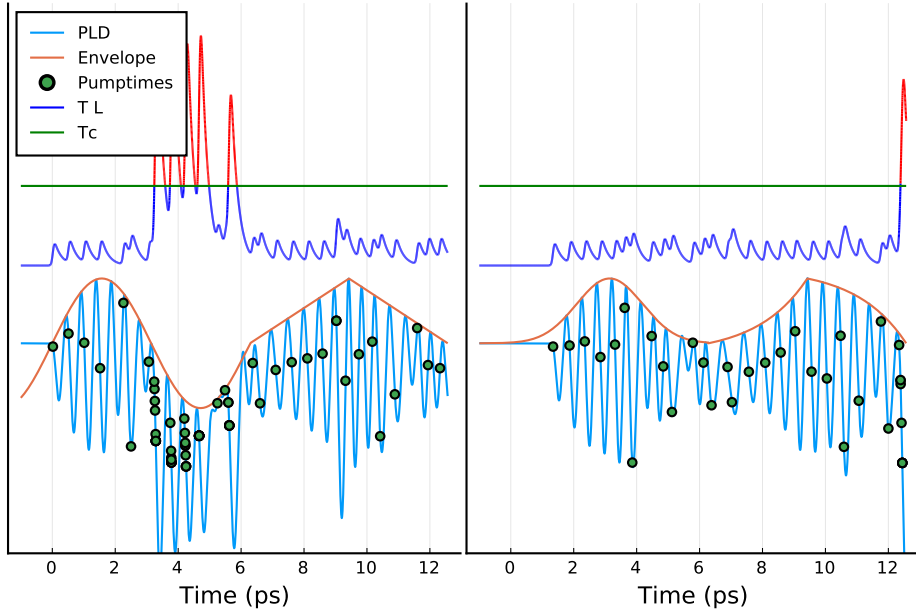


Figure 1.6: **Two examples of optimal control.** (a) One period of a sinusoid followed by a sawtooth with the same width and height. (b) Gaussian followed by an exponential and inverse exponential.

## 1.6 Conclusions

This chapter has shown that the coupling between the SDW and PLD through magnetostriction in Chromium is another prime example of a cross-order control, where in this case the perturbation applied by optical pulses to the SDW leads to an excitation in the PLD mode. Moreover, the slower dynamics of the PLD compared to the SDW opens up new behavior and additional dynamic control that would not be possible without the coupling. If the PLD would have dynamics on the same timescale as the SDW, changing its potential through excitation of the latter would not be very impactful since it would follow the minimum of the potential as fast as the excited SDW would change it.

As demonstrated by both the experiments and the theory, this allows for either increasing the oscillation amplitude dramatically (up to 450% the original value), or destroy it at a moment's notice, allowing for a shortcut to adiabaticity where the final state is at higher temperature than the original one.

Whether this can be exploited for technological means is probably a bit of a stretch, seen as XFELs are rather large. However, this understanding and demonstration of the perfect control of a couple order parameter could open the road to finding other similar situations with more technologically viable properties.